RESEARCH ARTICLE

An algebraic alternative for the accurate simulation of CO_2 Raman spectra

Marisol Bermúdez-Montaña[1] | **Miguel Carvajal[2,3]** |
Francisco Pérez-Bernal[2,3] | **Renato Lemus[4]** 🆔

[1]Facultad de Química, Universidad Nacional Autónoma de México, Aptdo. Postal 70-543, 04510 México, DF, México

[2]Dpto. Ciencias Integradas y Centro de Estudios Avanzados en Física, Matemáticas y Computación (CEAFMC); Universidad de Huelva, Unidad Asociada GIFMAN-UHU IEM-CSIC, Huelva, 21071, Spain

[3]Instituto Universitario "Carlos I" de Física Teórica y Computacional, Universidad de Granada, Granada, Spain

[4]Instituto de Ciencias Nucleares, Universidad Nacional Autónoma de México, Aptdo. Postal 70-543, 04510 México, DF, México

Correspondence
Renato Lemus, Instituto de Ciencias Nucleares, Universidad Nacional Autónoma de México, Aptdo. Postal 70-543, 04510 México, DF, México.
Email: renato@nucleares.unam.mx

Abstract

We present an accurate simulation of the Raman spectrum of the carbon dioxide molecule in the 1150–1500 cm^{-1} spectral range, comparing the results obtained using the three polyad schemes found in the literature of this molecule. The description of the molecule with the algebraic $U_1(2) \times U(3) \times U_2(2)$ local model encompasses both stretching and bending degrees of freedom. A detailed analysis of the Hamiltonian interactions for the three polyad schemes provides fittings with root mean square deviations in the range 0.14–0.20 cm^{-1}, involving 19 parameters taking into account the 178 experimental term energies found in the literature. Using a limited subset of 9 experimental transition moments, we optimize 5 partial derivatives of the mean polarizability and simulate the Raman spectrum of CO_2 for the three polyad schemes. Comparing the calculated results with the experimental spectrum, we obtain an overall good agreement for the three polyads. However, an inspection in detail of the spectrum seems to show a slight preference for polyad P_{212} albeit not due to the interaction characterizing the polyad but due to anharmonic effects and energy distribution. Finally, we assess the effect of the Fermi resonance over CO_2 Raman line intensities.

KEYWORDS
algebraic approach, carbon dioxide, polarizabilities, polyads, Raman spectrum

1 | INTRODUCTION

The measurement of carbon dioxide concentration in gas mixtures is currently carried out through spectroscopic techniques such as infrared, Raman, or nuclear magnetic resonance spectroscopy. For instance, the analysis of rovibrational transitions from laser absorption spectroscopy has been used in paleoclimatic studies for obtaining the CO_2 abundance in air bubbles found into ice cores from Antarctica.[1] An accurate measurement of CO_2 abundance is not only relevant for atmospheric sciences or paleoclimatology. In particular, Raman scattering is a useful tool for the quantitative diagnosis of combustion processes.[2,3] Molecular spectroscopy is also fundamental in the study of the chemistry of astronomical sources, for example, planetary atmospheres and the interstellar medium.[4]

The detection of molecular species in spectral surveys involves the obtention of experimental spectra and the succeeding analysis of the recorded spectra, making use of an appropriate theoretical model for the calculation of molecular (ro)vibrational levels. The model results should be accurate enough to allow for the prediction of levels beyond experimental access, improving the identification of the molecule into study in spectral surveys. In the present work, we study the vibrational structure of carbon dioxide with the aim of providing, through accurate predictions, term values filling some of the existing gaps in the available experimental frequencies. In addition to this, we check through the validity of the resulting wave functions making a comparison between experimental and simulated Raman spectra.

The present approach is based on an algebraic procedure carefully crafted to keep a link with the approach in configuration space. This feature makes possible the estimation of a potential energy surface from a set of optimized spectroscopic constants[5,6] that is in agreement with the surfaces obtained from works based on *ab initio* calculations or other theoretical procedures.[7–10] The need for accurate predicted data has fostered new developments in the algebraic approach to carbon dioxide vibrational structure.[5,6,11] The final result is a polyad-preserving theoretical model that provides a CO_2 vibrational description of spectroscopic quality.[11]

Polyad-based models have proved his efficiency in molecular spectral analysis for many molecular species.[12] In general, several polyad schemes are possible in accordance with different identification of resonances. In these situations, a convenient route consists in testing the provided wave functions through the transition intensities. The vibrational structure of the CO_2 molecule offers an excellent opportunity to carry out this kind of test because the analysis of the overtones and combinations suggest three polyads schemes. In this work, we simulate the CO_2 Raman spectrum using three different polyad schemes from the literature.[5,10,13,14] We compare simulated and experimental[2] results to reckon which polyad scheme is more suitable. In a previous work, polyad P_{212} was considered to generate a Raman spectrum simulation based on a spectroscopic description including 101 vibrational levels up to 9,600 cm^{-1} with a deviation of root mean square (*rms*) = 0.53 cm^{-1}[6] and involving 9 fitted transition moments.[15] The present simulated Raman spectrum involves the 178 known experimental term energies with deviations of rms = $0.14 - 0.20$ cm^{-1} up to 26,600 cm^{-1} based on the same 9 fitted transition moments for three different polyads. Hence, the predicted energies and wave functions are accurate enough to markedly improve the modeling of the CO_2 Raman spectrum allowing the best polyad scheme to be identified, a fact that provides possible targets for future experiments.

The material in this paper is organized as follows: in Section 2, the algebraic model for CO_2 is outlined. In Section 3, we briefly present the polyad-preserving model and the three polyad schemes considered, making special emphasis on the effect that the different interactions have on the energy spectrum. Section 4 includes a description of the procedure followed to calculate the Raman spectrum and the resulting simulations and a discussion of the polarizability derivatives effects on the spectrum. Finally, we set forth our concluding remarks in Section 5.

2 | ALGEBRAIC VIBRATIONAL HAMILTONIAN

Because our methodology to establish the vibrational Hamiltonian has already described in detail in Ref.,[15] here, we present only the salient ingredients of the model. The vibrational degrees of freedom of CO_2 are described in terms of curvilinear internal displacement coordinates. These coordinates are symmetry-adapted combinations of the internal displacement (valence) bond-stretching and angle-bending coordinates. The coordinates for the stretching degrees of freedom are

$$S_1 \equiv S_{\Sigma_g^+} = \frac{1}{\sqrt{2}}(\Delta r_1 + \Delta r_2), \quad S_3 \equiv S_{\Sigma_u^+} = \frac{1}{\sqrt{2}}(\Delta r_1 - \Delta r_2), \tag{1}$$

where $\Delta r_i = r_i - r_e$ with $i = 1, 2$ stands for the displacement of the i-th CO bond with respect to the equilibrium bond length r_e. The bending coordinates $\{S_{2a}, S_{2b}\}$ are defined as in Ref.[16] for linear molecules. Accordingly, the vibrational Hamiltonian $\hat{H}$ can be written as follows[17–20]

$$\hat{H} = \frac{1}{2}\tilde{\mathbf{P}}\mathbf{G}(\mathbf{S})P + V(\mathbf{S}), \tag{2}$$

where $\mathbf{S}$ and $\mathbf{P}$ are internal displacement coordinates and their conjugate momenta column vectors. The $\mathbf{G}(\mathbf{S})$ matrix

links internal and Cartesian coordinates and $V(\mathbf{S})$ is the Born–Oppenheimer potential, where the mass-dependent potential contribution has been neglected. The procedure to follow consists in the expansion of the $\mathbf{G(S)}$ matrix and the potential $V(\mathbf{S})$ as a Taylor series in terms of the $\mathbf{S}$ variables around the equilibrium configuration, truncating the expansion up to sixth order, which turns out to be enough to obtain high quality results. On the other hand, as explained in Ref.,[15] the curvilinear coordinates $(S_1, S_3, S_{2a}, and \ S_{2b})$ may be expanded in terms of rectilinear symmetry coordinates (normal coordinates) Q_α, $(\alpha = \Sigma_g^+, \Sigma_u^+, \Pi_{g,a}, \Pi_{g,b})$. Therefore, the Hamiltonian (2) is transformed to

$$\hat{H} = \hat{H}(\mathbf{P}, \mathbf{S}) \rightarrow \hat{H} = \hat{H}(\mathbf{p}, \mathbf{Q}), \quad (3)$$

where p are the conjugate momenta of Q. The Hamiltonian $\hat{H}(\mathbf{p}, \mathbf{Q})$ is rewritten in terms of bosonic creation and annihilation operators $(a_\alpha^\dagger, a_\alpha$, with $\alpha = \Sigma_{g/u}, \pm)$ in direct correspondence with the vibrational degrees of freedom. Correspondingly, the Hamiltonian (3) is expressed as

$$\hat{H}_P = \hat{H}_P(a_{\Sigma_g}^\dagger, a_{\Sigma_g}, a_{\Sigma_u}^\dagger, a_{\Sigma_u}, a_\pm^\dagger, a_\pm), \quad (4)$$

a transformation that allows for an algebraic representation with a straightforward identification of polyad-preserving interactions (resonances). It is worth recalling that the fundamental quantum number operators that define bending states are

$$\hat{\ell} = a_+^\dagger a_+ - a_-^\dagger a_- = \hat{n}_+ - \hat{n}_-,$$
$$\hat{n} = a_+^\dagger a_+ + a_-^\dagger a_- = \hat{n}_+ + \hat{n}_-, \quad (5)$$

where $\hat{n}$ and $\hat{\ell}$ are the number of bending quanta of excitation and the vibrational angular momentum, respectively.

Note that the relationship between spectroscopic parameters in (4) and the molecular geometry and force constants is preserved by the transformation from (2) to (4).[5,6] In order to simplify the vibrational Hamiltonian, only the relevant polyad-preserving interactions are kept. Thus, the Hamiltonian only includes resonances that couple vibrational states that comply with the preservation of the pseudo quantum number P, established by the polyad.

The resulting algebraic Hamiltonian may be diagonalized in a harmonic oscillator basis. This is the natural way to proceed when dealing with molecules with a strong normal mode character like CO_2. On the other hand, it is well known that the local mode scheme provides an alternative approach for the modeling of vibrational degrees of freedom, making use of local coordinates. The use of local coordinates for the CO_2 molecule, however, is not appropriate, first because polyads are defined in the framework of the normal mode scheme and also due to the fact that the force constants derived from optimized spectroscopic parameters of a polyad-preserving Hamiltonian defined in a local mode scheme may have unphysical values (see, e.g.,

Appendix B of Ref.[5]) unless a polyad-breaking Hamiltonian is applied, for example, by means of Van Vleck perturbation theory.[21] These two problems can be overcome by transforming the Hamiltonian (4) to a local algebraic representation through the following canonical transformation in the stretching coordinates

$$a_{\Sigma_g}^\dagger = \frac{1}{\sqrt{2}}(a_1^\dagger + a_2^\dagger), \quad a_{\Sigma_u}^\dagger = \frac{1}{\sqrt{2}}(a_1^\dagger - a_2^\dagger). \quad (6)$$

The bosonic operators $a_i^\dagger(a_i)$ are not local operators, but an isomorphism to the true local operators can be set up leading to a good approximation in the limit of weakly interacting oscillators.[22] Therefore, we can transform Hamiltonian (4) into a polyad-preserving Hamiltonian in a local picture making use of the canonical transformation (6).

Because the transformation (6) is canonical, it does not help by itself to gain a better description, the same energy levels are obtained. To further improve this description, we perform an anharmonization of the stretching local operators (see e.g., Refs.[6,23,24]) introducing the $U(2)$ operators $b_i^\dagger, b_i$:

$$a_i^\dagger \rightarrow b_i^\dagger, \ a_i \rightarrow b_i, \quad (7)$$

inducing the symmetry-adapted operators

$$a_{\Sigma_g}^\dagger \rightarrow b_{\Sigma_g}^\dagger \equiv \frac{1}{\sqrt{2}}(b_1^\dagger + b_2^\dagger), \ a_{\Sigma_u}^\dagger \rightarrow b_{\Sigma_u}^\dagger \equiv \frac{1}{\sqrt{2}}(b_1^\dagger - b_2^\dagger). \quad (8)$$

The creation (annihilation) operators $b_i^\dagger(b_i)$ are generators of a $U(2)$ dynamical algebra[25] and can be interpreted as ladder operators for Morse or Pöschl-Teller potential eigenstates $|j \ v_i\rangle$. Establishing the mapping $|j \ v_i\rangle \rightarrow |j \ n_i\rangle$,[26–28] in our approach, we take the matrix elements

$$b_i^\dagger |j \ n_i\rangle = \sqrt{(n_i + 1)(1 - (n_i + 1)/k_s)} \ |j \ n_i + 1\rangle,$$
$$b_i \ |j \ n_i\rangle = \sqrt{n_i(1 - n_i/k_s)} \ |j \ n_i - 1\rangle, \quad (9)$$

where n_i is the vibrational number of quanta, $n_i = 0, 1, 2, \ldots, j-1$, and $k_s = 2j+1$ is related to the depth of the internal bond stretching coordinates potential. Whereas the anharmonization (7) is valid also for 1D bending degrees of freedom in semi-rigid bent molecules,[23,24,29–34] the algebraic modeling of vibrational bending degrees of freedom in linear and non-rigid molecules is based on the $U(3)$ Lie algebra in order to encompass the coupling between rotational and vibrational degrees of freedom that occurs in degenerate and large amplitude bending modes.[5,6,11,15,35–40] In this latter case, we introduce the anharmonization procedure equivalent to Equation (7) through the mapping

$$a_\pm^\dagger \rightarrow b_\pm^\dagger \ a_\pm \rightarrow b_\pm, \quad (10)$$

with matrix elements[5]

$$
b_{\pm}^{\dagger}|[N]; n^{\ell}\rangle = \sqrt{\left(\frac{n \pm \ell}{2} + 1\right)\left(1 - \frac{n}{N}\right)}|[N]; (n+1)^{\ell \pm 1}\rangle,
$$

$$
b_{\pm}|[N]; n^{\ell}\rangle = \sqrt{\left(\frac{n \pm \ell}{2}\right)\left(1 - \frac{n-1}{N}\right)}|[N]; (n-1)^{\ell \mp 1}\rangle.
$$

$$(11)$$

The N parameter is the total number of bosons (vibrons) and labels the totally symmetric irreducible representation of the $U(3)$ Lie algebra that determines the dimension of the Hilbert space for the bending degree of freedom.

We stress that the anharmonization procedure (7) and (10) have proved to be crucial for the improvement of the spectroscopic description. Examples correspond to the BF_3 molecule[23] and the carbon dioxide itself.[6,11] In this work, we show that the wave functions are also dramatically improved, a fact that allows a high quality Raman simulation to be obtained.

3 | POLYAD PRESERVING HAMILTONIANS

Possible polyad schemes $P = \alpha \nu_1 + \beta \nu_2 + \gamma \nu_3$ are identified through the resonances appearing in the overtones and combinations. The frequencies for the fundamentals for the carbon dioxide are (in cm^{-1})

$$
\omega_1 = 1285.41; \ \omega_2 = 667.38; \ \omega_3 = 2349.14, \qquad (12)
$$

referred to Herzberg's notation.[41] The dominant resonance is the one identified by Fermi[42]: $\omega_1 \approx 2\omega_2$. This fixes the ratio $\alpha/\beta = 2$ but nothing can be said about α/γ. Taking $\alpha = \gamma$, the resulting polyad is

$$
\hat{P}_{212} = 2(\hat{\nu}_1 + \hat{\nu}_3) + \hat{\nu}_2. \qquad (13)
$$

This polyad has been used even though resonances associated with stretching interactions are not involved. A Darling–Dennison interaction is included in (13), although due to the fact that $2\omega_1 \neq 2\omega_3$, the contribution is expected not to be relevant. On the other hand, the splitting between the stretches is around 1,064 cm^{-1}, large enough to expect $\alpha \neq \gamma$.[22,43] The identification of the resonances $3\omega_1 \approx 2\omega_3$ and $4\omega_1 \approx 2\omega_3$ leads to polyad schemes[14],[44]–[52]

$$
\hat{P}_{213} = 2\hat{\nu}_1 + \hat{\nu}_2 + 3\hat{\nu}_3, \qquad (14)
$$

$$
\hat{P}_{214} = 2\hat{\nu}_1 + \hat{\nu}_2 + 4\hat{\nu}_3, \qquad (15)
$$

respectively. Polyad P_{214} involves higher order interactions that the ones included in P_{213}, a fact that may induce to preferred polyad P_{213}. However, the differences $4\omega_1 - 2\omega_3 \approx -443$ and $3\omega_1 - 2\omega_3 \approx 842$ suggest stronger resonances in P_{214}, and consequently, a preference to one of the polyads (14-15) is not obvious.

In this work, we consider the three polyad schemes (13-15) to simulate the Raman spectrum of CO_2[5,10,13,14] in order to elucidate the convenience to use one of the other. According to the algebraic approach, each scheme can be defined through the corresponding pseudo quantum number, corresponding to the eigenvalue of the operators given in (13-15), where $\hat{\nu}_i$ with $i = 1, 2, 3$ are normal number operators that in the present model are expressed in terms of symmetry-adapted operators as

$$
\hat{\nu}_1 = b_{\Sigma_g}^{\dagger} b_{\Sigma_g}; \ \hat{\nu}_2 = \hat{n}; \ \hat{\nu}_3 = b_{\Sigma_u}^{\dagger} b_{\Sigma_u}. \qquad (16)
$$

Hence, we define for each polyad an algebraic Hamiltonian that preserves the particular polyad. We start from a Hamiltonian in configuration space, obtain an algebraic realization (4) in a normal mode scheme, which in turn is transformed into a Hamiltonian in a local scheme through the transformations (6) and the anharmonization procedures (7) and (10). We express the three resulting algebraic Hamiltonians for the vibrational spectrum of the $^{12}CO_2$ molecule as follows:

$$
\hat{H}_{P_{212}} = \hat{H}_d + \hat{V}_{P_{212}}, \qquad (17)
$$

$$
\hat{H}_{P_{213}} = \hat{H}_d + \hat{V}_{P_{213}}, \qquad (18)
$$

$$
\hat{H}_{P_{214}} = \hat{H}_d + \hat{V}_{P_{214}}, \qquad (19)
$$

where the contribution $\hat{H}_d$ is common to the three polyad schemes and is given by

$$
\begin{aligned}
\hat{H}_d = &\sum_{i=1}^{3} \omega_i \hat{\nu}_i + \sum_{i \leq j} x_{ij}\{\hat{\nu}_i, \hat{\nu}_j\} + g_{22}\hat{l}^2 + f_{g/bb}\hat{F} \\
&+ x_{113}\{\hat{\nu}_1^2, \hat{\nu}_3\} + x_{133}\{\hat{\nu}_1, \hat{\nu}_3^2\} + x_{123}\hat{\nu}_2\{\hat{\nu}_1, \hat{\nu}_3\} \\
&+ \alpha_1^{sb}\{(\hat{n}_1 + \hat{n}_2), \hat{F}\} + \alpha_1^{s}\{(\hat{n}_1 + \hat{n}_2), \hat{D}_L + 2\hat{n}_1\hat{n}_2\} \\
&+ \alpha_2^{sb}\hat{n}(\hat{D}_L + 2\hat{n}_1\hat{n}_2) + f_{g/bb}^{[2]}\hat{F}^2.
\end{aligned} \qquad (20)
$$

The number of quanta for the local stretching degrees of freedom are

$$
\hat{n}_i = b_i^{\dagger}b_i; \ i = 1, 2. \qquad (21)
$$

In Equation (3), we have introduced the notation

$$
\{\hat{A}, \hat{B}\} = \frac{1}{2}(\hat{A}\hat{B} + \hat{B}\hat{A}), \qquad (22)
$$

where the symmetrization of non-commuting operators is necessary due to the anharmonization. In addition, the Fermi interaction $\hat{F}$, corresponding to the dominant resonance, is given by

$$
\hat{F} = b_{\Sigma_g}^{\dagger} b_+ b_- + H.c. \qquad (23)
$$

On the other hand, the interactions characterizing the Hamiltonians (17-19) have the explicit form:

$$
\hat{V}_{P_{212}} = f_{uu/gg}[b_{\Sigma_g}^{\dagger 2} b_{\Sigma_u}^2 + H.c.], \qquad (24)
$$

$$
\hat{V}_{P_{213}} = f_{uu/ggg}[b_{\Sigma_g}^{\dagger 3} b_{\Sigma_u}^2 + H.c.], \qquad (25)
$$

$$\hat{V}_{P_{214}} = f_{uu/gggg}[b_{\Sigma_g}^{\dagger 4} b_{\Sigma_u}^2 + H.c.]. \qquad (26)$$

The interaction (24) corresponds to the DD resonance, which in principle is not expected to be important as we have already pointed out.

The way we have recast the Hamiltonians (17-19) as $\hat{H}_d$ plus a polyad dependent term is advantageous when compared with the approach followed in Ref.[11] In the present case, we have managed to collect all the terms that are common to the three polyads in a single operator $\hat{H}_d$.

3.1 | Spectroscopic analysis

The Hamiltonians (17-19) may be interpreted as modeling three interacting oscillators: one 2D oscillator ($U[3]$ model, doubly degenerate bending degree of freedom) and two 1D Morse oscillators ($U[2]$ model, stretching degrees of freedom). Hence, the matrix representation of the Hamiltonian can be obtained in a $U_1(2) \times U(3) \times U_2(2)$ basis

$$|[N_s = 2j], [N_b]; n_1 n_2; n^\ell\rangle = |j n_1\rangle \otimes |j n_2\rangle \otimes |[N_b]; n^\ell\rangle. \qquad (27)$$

In practice, this basis is projected to obtain functions spanning irreducible representations of the $\mathcal{D}_{\infty h}$ point group.[53,54]

We present three fits to the 178 available experimental vibrational levels[14,15,44–47,51,55–60] for CO_2, making use of the Hamiltonians (17-19), associated with the polyads (13-15). In the three cases, the spectroscopic parameters were optimized with an iterative nonlinear least square method. The values of the boson numbers N_s and N_b were manually adjusted to $N_s = 159$ and $N_b = 150$ following Ref.[6]

We now proceed to study in detail the effect of the different interactions included in the Hamiltonian operators (17-19). To accomplish this goal, it is convenient to split the common term $\hat{H}_d$ in the following contributions:

$$\hat{H}_d = \hat{H}_0 + \hat{I}_{nD} + \hat{I}_{113} + \hat{I}_{123} + \hat{I}_{133} + \hat{I}_f^{[2]}, \qquad (28)$$

where

$$\hat{H}_0 = \sum_{i=1}^{3} \omega_i \hat{v}_i + \sum_{i \le j} x_{ij} \{\hat{v}_i, \hat{v}_j\} + g_{22}\hat{l}^2 + f_{g/bb}\hat{F} + \alpha_1^{sb}\{(\hat{n}_1 + \hat{n}_2), \hat{F}\}, \qquad (29)$$

whereas for the additional terms

$$\hat{I}_{nD} = \alpha_1^s\{(\hat{n}_1 + \hat{n}_2), (\hat{D}_L + 2\hat{n}_1\hat{n}_2)\} + \alpha_2^{sb}\hat{n}(\hat{D}_L + 2\hat{n}_1\hat{n}_2), \quad (30)$$

$$\hat{I}_{113} = x_{113}\{\hat{v}_1^2, \hat{v}_3\}, \quad \hat{I}_{123} = x_{123}\hat{v}_2\{\hat{v}_1, \hat{v}_3\}, \qquad (31)$$

$$\hat{I}_{133} = x_{133}\{\hat{v}_1, \hat{v}_3^2\}, \quad \hat{I}_f^{[2]} = f_{g/bb}^{[2]}\hat{F}^2. \qquad (32)$$

The usual parameter to measure the quality of the fits is given by the *rms* deviation defined as

$$rms = \sqrt{\frac{\sum_{i=1}^{N_e} (E_{exp}^{(i)} - E_{th}^{(i)})^2}{(N_e - N_p)}}, \qquad (33)$$

where N_e is the number of experimental energies $E_{exp}^{(i)}$ taken into account ($N_e = 178$), $E_{th}^{(i)}$ are the energies computed by the model, and N_p stands for number of parameters involved. However, when different fits of the same high quality are compared, like in CO_2, a more convenient quantity to assess the effects of the different interactions is the sum of the squared residuals σ^2 defined as

$$\sigma^2 = \sum_{i=1}^{N_e} (E_{exp}^{(i)} - E_{th}^{(i)})^2, \qquad (34)$$

which is more sensitive to the fits. To accomplish the fits, we start introducing the contribution $\hat{H}_0$ common to the three polyads. The obtained fit, together with the deviation σ^2, is displayed in the first row of Table 1. There is a reasonable agreement with the experiment, with $\sigma^2 \simeq 50$ cm^{-1} ($rms \simeq 0.5$ cm^{-1}), where we include the Fermi interaction. As a next step, the interactions characterizing the three polyads $\hat{V}_\alpha$, with $\alpha = 212$, 213, and 214, were taken into account. The effect of these resonances was only noticeable in the 213 case, reducing σ^2 to half its value, as shown in the second row of Table 1. Including the $\hat{I}_{nD}$ interactions (30) instead of the $\hat{V}_\alpha$ resonances, deviations with $\sigma^2 \simeq 10$cm^{-2} ($rms = 0.25$ cm^{-1}) were reached. Then we proceeded including the interactions $\hat{I}_{113}$, $\hat{I}_{123}$, $\hat{I}_{133}$, and $\hat{I}_f^{[2]}$ (31-32), which contribute to further refine the agreement with the experimental spectrum (Table 1). A graphical representation of the results obtained in this analysis is shown in Figure 1. We conclude that Hamiltonian,

$$\hat{H} = \hat{H}_0 + \hat{I}_{nD} + \hat{I}_{123}, \qquad (35)$$

provides a reasonable description of the CO_2 vibrational spectrum, with a *rms* deviation of 0.183 cm^{-1} for $\hat{H}_{P_{212}}$, 0.242 cm^{-1} for $\hat{H}_{P_{213}}$, and 0.234 cm^{-1} for $\hat{H}_{P_{214}}$. However, in order to provide an appropriate assessment of the polyad schemes, in this work we consider the full 19 parameter Hamiltonians (17-19), obtaining $rms = 0.145$ cm^{-1} for $\hat{H}_{P_{212}}$, 0.140 cm^{-1} for $\hat{H}_{P_{213}}$, and 0.202 cm^{-1} for $\hat{H}_{P_{214}}$. There is a slight improvement for the polyad schemes P_{213} and P_{214} with respect to our former work.[11]

It is well known that a good fit to the experimental energy spectrum does not necessarily guarantee that the obtained wave functions have the necessary physical ingredients to describe the model under study.[61] A test of the wave functions quality is therefore of great help to evaluate the model results. This situation will be discussed in detail in the next section, where the modeling of the CO_2 Raman spectrum is introduced. The calculated energies and the residuals when compared with the experimental spectrum for the three polyad schemes are included as Supporting Information for this work.

TABLE 1 Values of σ^2 (34) in cm^{-2} units obtained in the fits to the $N_e = 178$ available experimental term energies with Hamiltonian operators (17-19) for different parameterizations

N_p	Hamiltonian	σ^2 (cm^{-2})		
		P_{212}	P_{213}	P_{214}
12	$\hat{H}_0$	49.8681	46.9326	57.1134
13[a]	$\hat{H}_0 + \hat{V}_\alpha$	45.1744	28.0713	50.6968
14	$\hat{H}_0' = \hat{H}_0 + \hat{I}_{nD}$	7.14401	12.1092	13.019
15	$\hat{H}_0' + \hat{I}_{123}$	5.46412	9.55302	8.9437
16	$\hat{H}_0' + \hat{I}_{113} + \hat{I}_{123}$	5.10786	7.97162	7.29859
17	$\hat{H}_0'' = \hat{H}_0' + \hat{I}_{113} + \hat{I}_{123} + \hat{I}_{133}$	5.03384	7.32553	6.5162
18	$\hat{H}_0'' + \hat{I}_f^{[2]}$	3.67326	3.42145	6.48328
19[a]	$\hat{H}_0'' + \hat{V}_\alpha + \hat{I}_f^{[2]}$	3.33082	3.12642	6.48365
	$rms = \sqrt{\sigma^2/(N_e - N_p)}$ (cm^{-1})	0.1447	0.1402	0.2019

Note. The standard *rms* value is also provided for the case including 19 parameters. [a]α labels each column P_{212}, P_{213} and P_{214}, whereas the $\hat{V}_\alpha$ are defined in (13), (14) and (15).
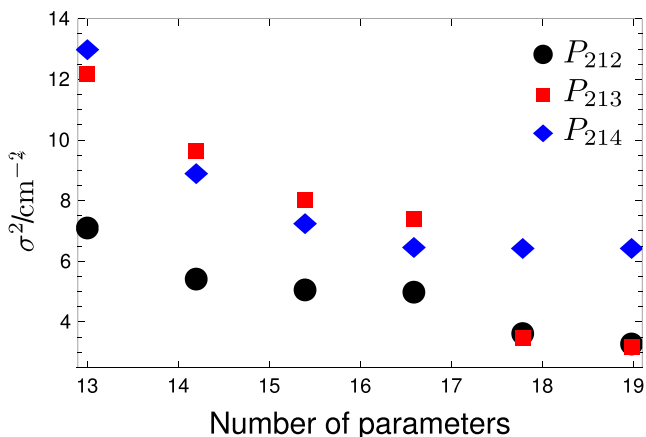

FIGURE 1 Deviation σ^2 defined in (34). The different interactions added to the initial Hamiltonian H_0 can be found in Table 1. The deviation attained for each Hamiltonian is plotted as a function of the total number of spectroscopic parameters taken into account

4 | RAMAN SPECTRUM SIMULATION

We model the vibrational Raman spectrum of CO_2 from the vibrational eigenenergies and eigenstates computed in Section 3, including transitions with term values in the (1150, 1500) cm^{-1} region. Beyond this region, Raman transitions are not observed. In fact, at temperature 1,743 K, the intervals (500-1150) and (1500-2000) cm^{-1} were explored without any intensity registered. The line intensities are calculated using the differential cross section, expressed in the SI system, for the trace scattering of a gas sample at thermal equilibrium[62]

$$\left(\frac{\partial\sigma}{\partial\Omega}\right)_{i \to f}^{\text{trace}} = \left(\frac{\pi}{\epsilon_0}\right)^2 \frac{(\nu_0 + \nu_i - \nu_f)^4}{Z_{vib}(T)} g_{if} |M_{if}|^2 \exp\left(\frac{-hc\nu_i}{k_B T}\right), \quad (36)$$

where ϵ_0 is the vacuum permitivity, ν_0 is the wavenumber of the exciting radiation ($\nu_0 = 19730$ cm^{-1} in Ref.[2]), ν_i and ν_f are the term values of the initial and final states, and g_{if} is the vibrational degeneracy of the transition. The vibrational partition function at a temperature (T) of

the gas sample is computed as a direct sum, $Z_{vib}(T) = \sum_j g_j e^{-\nu_j/k_B T}$, where g_j is the degeneracy of the states with ν_j energy. The vibrational term values ν_j considered in the vibrational partition sum are computed in each polyad scheme, by means of the Hamiltonians (17-19), up to 26,000 cm^{-1}. In Table S1, we provide values of the partition function for each polyad scheme and at different temperatures. The Raman transition intensities are mainly due to the totally symmetric mean molecular polarizability $\bar{\alpha}_{\Sigma_g^+} = \bar{\alpha}$, and the integral of the transition moment $M_{if} = \langle \nu_i | \bar{\alpha} | \nu_f \rangle$ can be calculated from the polarizability expressed as a function of the internal coordinates and making use of the vibrational states $|\nu_i\rangle$ and $|\nu_f\rangle$ obtained in Section 3.

In this work, we expand the mean polarizability in terms of the curvilinear symmetry coordinates S_α up to cubic order as follows:

$$\begin{aligned}
\bar{\alpha}_{\Sigma_g^+} = \bar{\alpha}_0 &+ \left(\frac{\partial\bar{\alpha}}{\partial S_{\Sigma_g^+}}\right)_0 S_{\Sigma_g^+} + \frac{1}{2}\left(\frac{\partial^2\bar{\alpha}}{\partial S_{\Sigma_g^+}^2}\right)_0 S_{\Sigma_g^+}^2 + \frac{1}{2}\left(\frac{\partial^2\bar{\alpha}}{\partial S_{\Sigma_u^+}^2}\right)_0 S_{\Sigma_u^+}^2 \\
&+ \frac{1}{2}\left(\frac{\partial^2\bar{\alpha}}{\partial S_{2a}^2}\right)_0 (S_{2a}^2 + S_{2b}^2) + \frac{1}{2}\left(\frac{\partial^3\bar{\alpha}}{\partial S_{\Sigma_g^+}\partial S_{2a}^2}\right)_0 \\
&\times S_{\Sigma_g^+}(S_{2a}^2 + S_{2b}^2) + \frac{1}{2}\left(\frac{\partial^3\bar{\alpha}}{\partial S_{\Sigma_g^+}\partial S_{\Sigma_u^+}^2}\right)_0 S_{\Sigma_g^+} S_{\Sigma_u^+}^2, \quad (37)
\end{aligned}$$

where the values of the different polarizability derivatives can be determined either from a fit of experimental transition moments[62,63] or from *ab initio* calculations.[64,65]

We use the Raman spectrum as a probe to check the quality of the wave functions resulting from the fit to the experimental spectrum using each polyad scheme separately. In order to do so, we carry out spectral simulations for each case and compare the obtained results with the experimental Raman spectrum of CO_2 at $T = 1743$ K. Thus, we have to calculate the matrix elements of the mean molecular polarizability $\bar{\alpha}$ for the eigenstates of Hamiltonians $H_{P_{212}}$, $H_{P_{213}}$, and $H_{P_{214}}$ (17-19). The approach we follow is very similar to the one introduced for the calculation

of the Hamiltonian matrix elements. We define an algebraic representation of the $\bar{\alpha}$ operator in terms of bosonic $a_\alpha^\dagger$, a_α, with $\alpha = \Sigma_{g/u}, \pm$. Then, we apply the canonical transformation (6), and we perform the anharmonization procedures (7) and (10). In this way, the matrix elements of the $\bar{\alpha}$ in the local basis (27) are well defined, and the transition moments $M_{if} = \langle v_i | \bar{\alpha} | v_f \rangle$ can be calculated using the expansion (4).

Therefore, we compute Raman intensity values using Equation (36), the eigenfunctions obtained in the different fits performed and the partial derivatives of the mean polarizability from the power expansion (4), whose values are obtained from a fit to the available experimental matrix elements $|M_{if}^{(exp)}|$.[62,66] We show in Table 2 the experimental transition moment values and the calculated ones. The first three columns provide the experimental transition frequencies, the initial and final state assignments, and the experimental molecular polarizability transition moments $|M_{if}^{(exp)}|$.[62,66] For the sake of comparison, we include the results obtained in previous works using rectilinear[67] (fourth column) and curvilinear[15] (fifth column) coordinate approximations to the symmetry coordinates. The present work results for the polyad schemes, P_{212}, P_{213}, and P_{214}, labeled as $|M_{if}^{(calc)}|$, are shown in the sixth, seventh, and eighth columns, respectively. These were computed by fitting the first 9 experimental transition moments minimizing a *rms* deviation between experimental $|M_{if}^{(exp)}|$ and calculated $|M_{if}^{(calc)}|$ transition moments defined as[67]
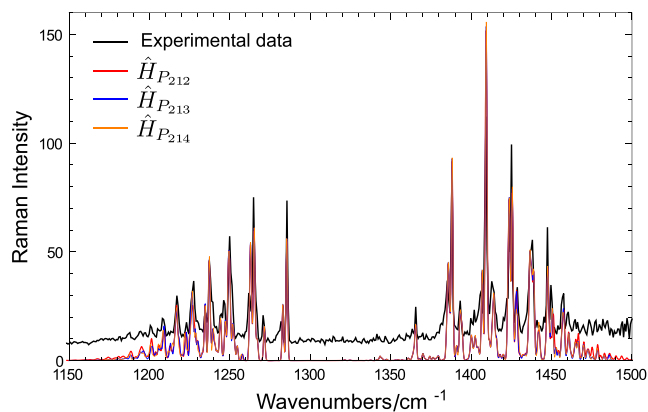

FIGURE 2 Experimental (black line) and calculated Raman spectrum of CO_2 in the $1,150 - 1,500$ cm^{-1} range. The predicted transition lines are obtained making use of the eigenenergies and eigenfunctions of the algebraic Hamiltonians $\hat{H}_{P_{212}}$ (red line), $\hat{H}_{P_{213}}$ (blue line), and $\hat{H}_{P_{214}}$ (orange line)

$$rms = \sqrt{\sum_\beta \left(\log |M_\beta^{(exp)}| - \log |M_\beta^{(calc)}| \right)^2}. \quad (38)$$

It is worth to notice that the *rms* values obtained in this work are slightly higher than the values reported in Ref.,[15] but the differences are very small as can be seen in the last row of Table 2.

The simulated Raman spectrum in the wave number range $1,150 - 1,500$ cm^{-1} is compared with the experimental one in Figure 2. We display a zoom of the previous spectrum in the spectral ranges around $1,180 - 1,280$ cm^{-1} in Figure 3 and $1,360 - 1,500$ cm^{-1} in Figure 4. It can be

TABLE 2 Experimental and calculated transition moments $|M_{if}| = |\langle v_i | \bar{\alpha} | v_f \rangle|$ of the mean polarizability of CO_2 in the three polyad schemes

ν (cm^{-1})[a]	$|v_i\rangle \rightarrow |v_f\rangle$ transition[b]	$|M_{if}^{(exp)}|$[c]	$|M_{if}|$[d]	$|M_{if}|$[e]	$|M_{if}^{(calc)}|$[f]		
					P_{212}	P_{213}	P_{214}
1285.41	$|000; \Sigma_g^+\rangle \rightarrow |020; \Sigma_g^+\rangle$	5.58	5.58	5.59	5.610	5.620	5.610
1388.18	$|000; \Sigma_g^+\rangle \rightarrow |100; \Sigma_g^+\rangle$	6.79	6.79	6.89	6.910	6.890	6.890
2548.37	$|000; \Sigma_g^+\rangle \rightarrow |120; \Sigma_g^+\rangle$	0.088	0.089	0.084	0.083	0.083	0.083
2671.14	$|000; \Sigma_g^+\rangle \rightarrow |200; \Sigma_g^+\rangle$	0.114	0.110	0.116	0.118	0.118	0.117
2797.14	$|000; \Sigma_g^+\rangle \rightarrow |120; \Sigma_g^+\rangle$	0.026	0.026	0.026	0.026	0.026	0.026
4673.33	$|000; \Sigma_g^+\rangle \rightarrow |002; \Sigma_g^+\rangle$	0.050[h]	0.050	0.050	0.050	0.050	0.050
1265.09	$|010; \Pi_u\rangle \rightarrow |030; \Pi_u\rangle$	5.4	5.41	5.41	5.420	5.420	5.420
1409.48	$|010; \Pi_u\rangle \rightarrow |110; \Pi_u\rangle$	7.2	6.95	7.060	7.060	7.040	7.050
2514.08	$|010; \Pi_u\rangle \rightarrow |130; \Pi_u\rangle$	0.095	0.107	0.098	0.098	0.098	0.098
2671.98	$|010; \Pi_u\rangle \rightarrow |210; \Pi_u\rangle$	...	0.102	0.109	0.112	0.012	0.111
2833.29	$|010; \Pi_u\rangle \rightarrow |130; \Pi_u\rangle$	≤0.03	0.019	0.016	0.016	0.016	0.016
rms[g]		-	0.135	0.060	0.075	0.075	0.072

Note. The results obtained in this work are also compared with those computed in previous works. [a]Experimental transition wavenumber values from Ref.[62] [b]Initial and final vibrational states are labeled by the ket $|v_1 v_2 v_3; \Gamma\rangle$ where (v_1, v_2, v_3) are the quantum numbers in the normal-mode representation and Γ is the vibrational wavefunction symmetry. [c]Experimental transition moment values from Ref.[62] in 10^{-42}CV^{-1}m^2 units, otherwise is indicated. Only the first nine transitions were involved in the fit. [d]Calculated transition moments in 10^{-42}CV^{-1}m^2 units reported in.[67] [e]Calculated transition moments in 10^{-42}CV^{-1}m^2 units reported in.[15] [f]Fitted transition moments in 10^{-42}CV^{-1}m^2 units obtained for the different polyad schemes considered in this work. [g]The definition of *rms* is given in Eq. (38). [h]Experimental value from Ref.[66]
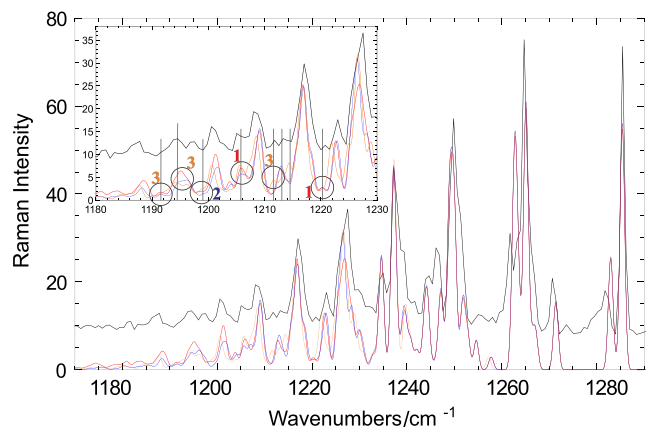
FIGURE 3 Zoom left for the experimental and calculated Raman spectrum of CO_2. The predicted transition lines are obtained making use of the eigenenergies and eigenfunctions of the algebraic Hamiltonians $\hat{H}_{P_{212}}$ (red line), $\hat{H}_{P_{213}}$ (blue line), and $\hat{H}_{P_{214}}$ (orange line). In the box are pointed the main differences, the number correspond to the polyad which has a better behaviour
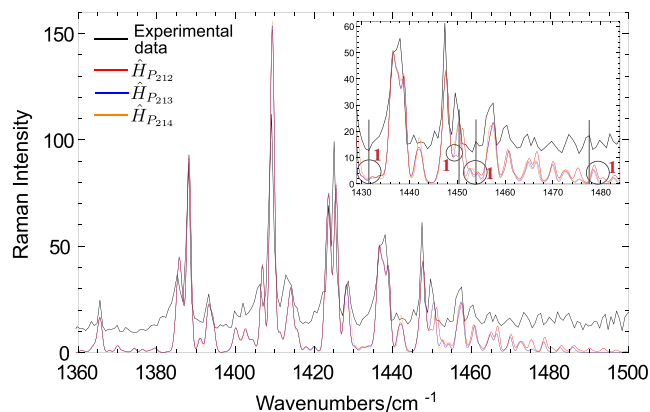

FIGURE 4 Zoom right for the experimental and calculated Raman spectrum of CO_2. The predicted transition lines are obtained making use of the eigenenergies and eigenfunctions of the algebraic Hamiltonians $\hat{H}_{P_{212}}$ (red line), $\hat{H}_{P_{213}}$ (blue line), and $\hat{H}_{P_{214}}$ (orange line). In the box are pointed the main differences, the number correspond to the polyad which has a better behaviour

easily noticed that the overall spectra are similar, and only slight differences appear lying in the tails.

Fitting the experimental transition moment values in Table 2, we obtain the derivatives of $\bar{\alpha}$ with respect to curvilinear symmetry coordinates, S_{α}. The obtained values are shown in the upper rows of Table 3. As we have done for the transition moments, we include the values reported by Tejeda et al.,[62] the results obtained using a linear approximation for the symmetry coordinates[67] and the values obtained with curvilinear symmetry coordinates.[15] In the lower rows of Table 3, we include the derivatives calculated in the corresponding dimensionless normal coordinates. The difference between the present work

results and the ones obtained by Tejeda et al.[62] can be due to the different approaches followed to calculate the eigenstates and to extract the partial derivative values from the experimental transition moments. In the latter case, Tejeda et al.[62] used perturbation theory to map experimental transition moments and derivative values. The difference between our results and the results from Ref.,[67] where a rectilinear coordinates approximation was used, is due to the considerable nonlinear effects in the polarizability, specially when only the bending coordinates are involved. In the case of the results obtained in Ref.,[15] using the same approach than in the present work, the differences stem from the different and more accurate fits performed in the present work, that include the whole set of experimental energies available in Ref.,[11] and consequently, we expect to have a more accurate set of eigenstates, even though our results in Tables 2 and 3 deviate from the values reported by Tejeda et al.[62]

The results presented in Table 3, obtained with different approaches to the partial derivatives of the mean polarizability, and their influence in the computed Raman spectrum deserve a discussion. With this aim, we compare in Figure 5 the experimental spectrum with the calculated spectrum using the different sets of derivatives in Table 3. We split the figure in two panels, defined for the same spectral ranges shown in Figures 3 and 4. As we include the results of Ref.,[15] we will only consider the present results for the polyad scheme P_{212}. The depicted simulations were computed using the present work eigenstates for polyad scheme P_{212} and different sets of partial derivatives of the mean polarizability: (a) the derivatives of Ref.[62] (blue lines); (b) the derivatives presented in Ref.[15] (orange lines); and (c) the derivatives obtained in this work (red lines). It is easily noticed how similar the different simulation results are.

Another aspect that it is also worth clarifying when comparing the output of different calculation is the effect of the number of transitions included in the calculation. For each polyad scheme, the calculated transitions falling in the interval $(1150, 1500)$ cm^{-1} are taken from the list of predicted energies up to 26,000 cm^{-1} (see Supporting Information). The differences between the pairs of calculated energy levels, considering the selection rules, provide the transition frequencies, and the transition moments are computed from the wave functions of the pairs. Following this approach, in the present work, the number of transitions included in the simulated spectrum is of the order of 18,000, whereas in Ref.,[15] only 800 lines were taken into account. A question which arises is concerned with the effect of the number of lines included. In other words, it is not clear whether the enhancement of the agreement with the experimental spectrum is due to the increase of the number of transitions or to the improved

TABLE 3 Partial derivatives of the CO_2 mean polarizability with respect to curvilinear symmetry coordinates and to dimensionless normal coordinates

Derivative (units)[a]	Tejeda[b]	Linear[c]	Nonlinear[d]	This work[e]		
				P_{212}	P_{213}	P_{214}
$\left(\dfrac{\partial \bar{\alpha}}{\partial S_{\Sigma_g^+}}\right)_0$ $(10^{-30}\text{CV}^{-1}\text{m})$	3.15±0.02	3.15	3.181	3.20	3.19	3.19
$\left(\dfrac{\partial^2 \bar{\alpha}}{\partial S^2_{\Sigma_g^+}}\right)_0$ (10^{-20}CV^{-1})	2.9±0.2	2.549	2.634	2.61	2.62	2.63
$\left(\dfrac{\partial^2 \bar{\alpha}}{\partial S^2_{\Sigma_u^+}}\right)_0$ (10^{-20}CV^{-1})	0.5±0.1[f]	0.447	0.448	0.465	0.445	0.445
$\left(\dfrac{\partial^2 \bar{\alpha}}{\partial S^2_{2a}}\right)_0$ (10^{-20}CV^{-1})	0.36±0.06	0.8395	−0.060	−0.235	−0.258	−0.197
$\left(\dfrac{\partial^3 \bar{\alpha}}{\partial S_{\Sigma_g^+} \partial S^2_{2a}}\right)_0$ $(10^{-10}\text{CV}^{-1}\text{m}^{-1})$	−1.7±0.03	−1.21	−1.2	−1.11	−1.10	−1.13
Dimensionless normal coordinates[g]						
$\bar{\alpha}'_1 (10^{-42}\text{CV}^{-1}\text{m}^2)$	12.43±0.07	12.44	12.56	12.46	12.44	12.43
$\bar{\alpha}''_{11} (10^{-42}\text{CV}^{-1}\text{m}^2)$	0.45±0.03	0.398	0.411	0.396	0.398	0.399
$\bar{\alpha}''_{33} (10^{-42}\text{CV}^{-1}\text{m}^2)$	0.15±0.04	0.144	0.144	0.153	0.146	0.146
$\bar{\alpha}''_{+-} (10^{-42}\text{CV}^{-1}\text{m}^2)$	2.81±0.08	1.925	2.12	1.85	1.81	1.91
$\bar{\alpha}'''_{1+-} (10^{-42}\text{CV}^{-1}\text{m}^2)$	−0.06±0.02	−0.110	−0.06	−0.075	−0.076	−0.073

Note. The second, third and fourth columns include the values obtained by Tejeda et al.,[62] and the results previously obtained using a linear[67] and nonlinear[15] approximation to the symmetry coordinates. The final three columns are the results obtained in the present work for the three polyad schemes under study. [a] Partial polarizability derivatives as defined in Equation (4). [b] Values reported in Ref.[62] [c] Values obtained using a rectilinear coordinate approximation for the symmetry coordinates from Ref.[67] [d] Values obtained using a curvilinear coordinate approximation for the symmetry coordinates from Ref.[15] [e] Present work results from the fits to experimental polarizability transition moments shown in Table 2. [f] Best choice of the two values provided in Ref.,[62] according to the *ab initio* CCSD(T) value of Ref.[65] [g] Polarizability derivatives in terms of dimensionless normal coordinates as defined in Ref.[62]
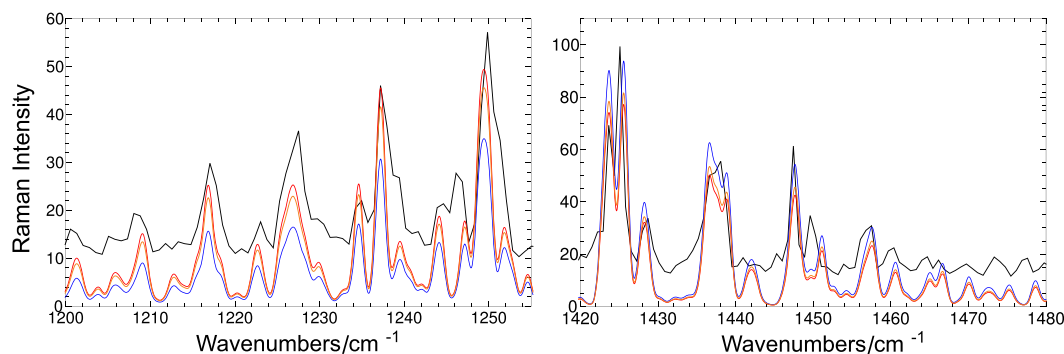
FIGURE 5 Experiment (black line) and simulated Raman spectra of CO_2 using different values of the derivatives in (4): the given in Ref.[62] (blue line), the computed in Ref.[15] (orange line) and the optimized set obtained in this work for the polyad scheme P_{212} (red line)

wave functions. To answer this question, in Figure 6, we compare the results presented in Ref.[15] and the present results using the polyad scheme P_{212} and Hamiltonian (17). In this figure, the experimental spectrum is depicted using black lines, and the present work full calculation, already plotted in Figure 2, is depicted using red lines. To ascertain the origin of the improvement in the calculated spectrum, we also include in Figure 6 the following calculations: the results from Ref.[15] (blue lines) and the results of the present work limiting the transitions to those considered in Ref.[15] (orange lines). Comparing these two latter simulations, the blue lines versus the orange ones, we conclude that the improved set of eigenstates used in

this work is responsible for the enhancement obtained in the Raman simulation. Comparing red and orange lines, it can be easily noticed that the effect of an increase in the number of transitions included in the calculation is relevant only along the spectrum tails, where no high intensity transitions are present.

Considering the calculated frequency positions and line intensities, we conclude that the Raman simulations displayed in this work offer a noticeable improvement in the simulation of CO_2 Raman spectrum at 1,743 K with respect to Ref.[15] results. This cannot be explained by the larger number of transitions involved in the simulation but to the improvement in the quality of the wave functions.
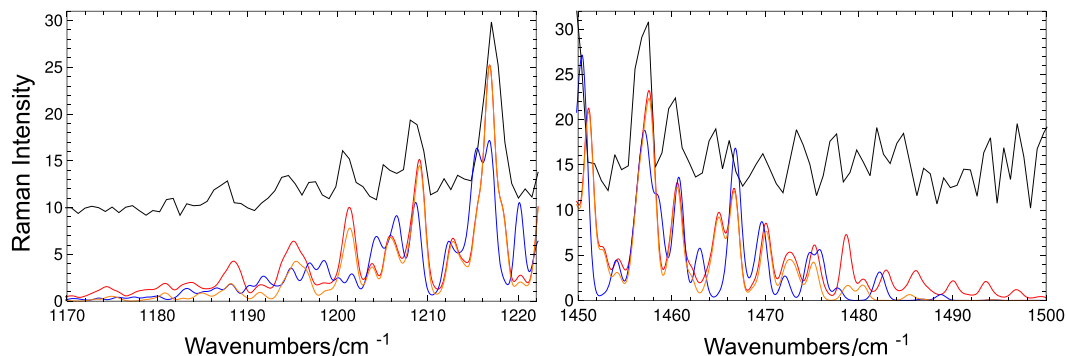
FIGURE 6 Comparison of the experimental Raman spectrum (black lines) of CO_2 to the following three simulations: a) the present work for polyad scheme P_{212} (red line); b) the one of Ref.[15] (blue line); and c) an alternative one, that encompass the same number of transitions than Ref.[15] but using the eigenfunctions of present work (orange lines)
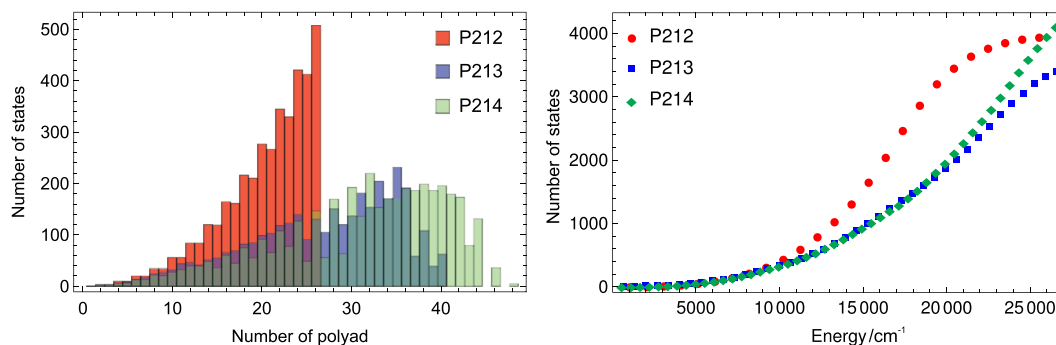

FIGURE 7 Left: histogram of number of states by number of polyad. Right: accumulative density of states with respect to the energy for each polyad scheme

In the framework of our work, it is clear that a key point is the inclusion of the Fermi resonance. To elucidate the effect of the resonances involving the stretching modes characterizing the polyads, we compared for each polyad the Raman spectrum generated by the wave functions using the common Hamiltonian H_d and the complete Hamiltonian $\hat{H}_d + V_P$. The result is that both spectra turn out to be practically the same with minimum changes from the quantitative point of view. This fact supports the conclusion that the resonances characterizing the polyads are practically irrelevant and that the common contribution $\hat{H}_d$ establishes the physical features of the wave functions. This fact may induce to think that the three polyad schemes provide the same Raman spectrum. This is in fact the case concerning the overall spectrum but not in details. In Figures 3 and 4, the Raman spectrum predicted by the three polyads schemes is depicted. Even though the general trend is similar for the three polyads, some differences are evident. In the same figures, a zoom of the spectrum is depicted, where we have pointed out with circles the regions where differences are manifested. From qualitative considerations, we have added a tentative number to the best polyad description. This assignment may indicate that the best spectrum is provided by the

P_{212} polyad scheme, although this is questionable due to the lack of a quantitative criterion at this level of accuracy. However, histograms corresponding to the density of states with respect to the polyad number as well as the accumulative density with respect to the energy for each polyad scheme displayed in Figure 7 show quite different behavior. Whereas for polyad P_{212}, a uniform increase of states is manifested up to 26,000 cm^{-1}, in the other two polyads a maximum is reached. This fact is reflected in the partition function presented in the Supporting Information where the convergence of the direct sum of the vibrational partition function seems that it is not reached for polyads schemes P_{213} and P_{214}[68] despite a considerable number of states are taken into account. We believe that anharmonicity reflected in the Raman spectrum together with the uniform increase of states makes polyad P_{212} a better polyad scheme. Although this conclusion is not definitive, we consider the need to discuss these differences originated from anharmonic effects because the expected description in terms of a harmonic oscillator basis is independent of the polyad scheme as long as the Hamiltonian is taken to be $\hat{H} = \hat{H}_d$. This fact leads to the conclusion that the anharmonic effects as well as
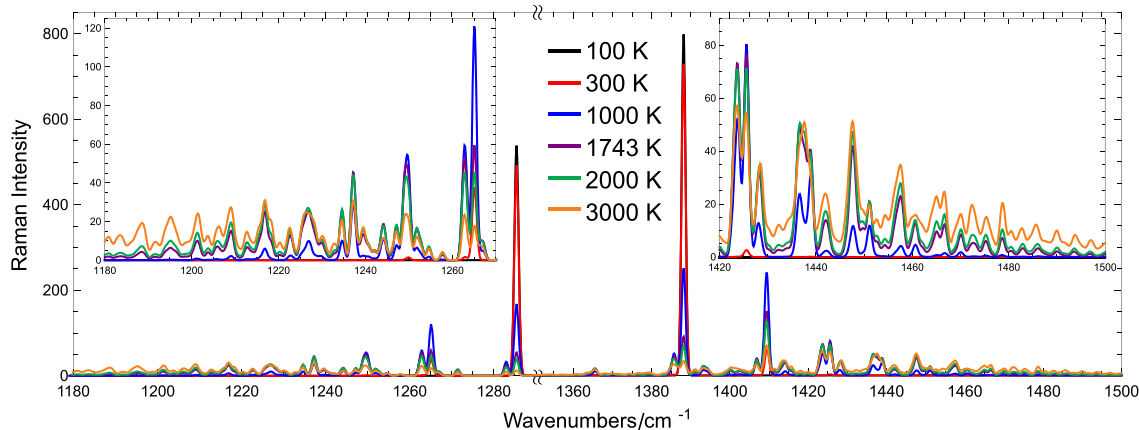
FIGURE 8 Simulated Raman spectrum of CO_2 at 100, 300, 1000, 1743, 2000 and 3000 K using the eigenenergies and eigenfunctions of the algebraic Hamiltonian $\hat{H}_{P_{212}}$. [Colour figure can be viewed at wileyonlinelibrary.com]

TABLE 4 Raman intensity obtained for some transitions using the Hamiltonian $\hat{H}_{P_{212}}$ (17) (left part) and the Hamiltonian $\hat{H}_{NF}$ (4.1) (right part)

Hamiltonian $\hat{H}_{P_{212}}$, rms=0.14 cm^{-1}			Non-Fermi Hamiltonian $\hat{H}_{NF}$, rms= 25.76 cm^{-1}		
$\|v_i\rangle \to \|v_f\rangle$ transition	$\nu_f - \nu_i$ (cm^{-1})	Raman Intensity	$\|v_i\rangle \to \|v_f\rangle$ transition	$\nu_f - \nu_i$ (cm^{-1})	Raman Intensity
$\|0; 000; \Sigma_g^+\rangle \to \|2; 020; \Sigma_g^+\rangle$	1285.39	4.112	$\|0; 000; \Sigma_g^+\rangle \to \|2; 100; \Sigma_g^+\rangle$	1249.22	10.80
$\|0; 000; \Sigma_g^+\rangle \to \|2; 100; \Sigma_g^+\rangle$	1388.28	6.667	$\|0; 000; \Sigma_g^+\rangle \to \|2; 020; \Sigma_g^+\rangle$	1387.96	0.1419
$\|2; 020; \Sigma_g^+\rangle \to \|4; 120; \Sigma_g^+\rangle$	1262.87	2.203	$\|2; 020; \Sigma_g^+\rangle \to \|4; 120; \Sigma_g^+\rangle$	1244.44	3.682
$\|2; 100; \Sigma_g^+\rangle \to \|4; 200; \Sigma_g^+\rangle$	1283.06	1.898	$\|2; 100; \Sigma_g^+\rangle \to \|4; 200; \Sigma_g^+\rangle$	1265.19	7.438
$\|2; 020; \Sigma_g^+\rangle \to \|4; 200; \Sigma_g^+\rangle$	1385.95	2.888	$\|2; 100; \Sigma_g^+\rangle \to \|4; 120; \Sigma_g^+\rangle$	1383.18	0.0488
$\|2; 100; \Sigma_g^+\rangle \to \|4; 120; \Sigma_g^+\rangle$	1408.91	3.645	$\|2; 020; \Sigma_g^+\rangle \to \|4; 040; \Sigma_g^+\rangle$	1408.64	0.1707
$\|4; 120; \Sigma_g^+\rangle \to \|6; 140; \Sigma_g^+\rangle$	1244.31	1.002	$\|4; 040; \Sigma_g^+\rangle \to \|6; 140; \Sigma_g^+\rangle$	1239.66	1.044
$\|4; 120; \Sigma_g^+\rangle \to \|6; 300; \Sigma_g^+\rangle$	1267.28	0.5805	$\|4; 120; \Sigma_g^+\rangle \to \|6; 220; \Sigma_g^+\rangle$	1256.6	2.329
$\|4; 200; \Sigma_g^+\rangle \to \|6; 300; \Sigma_g^+\rangle$	1271.39	1.144	$\|4; 200; \Sigma_g^+\rangle \to \|6; 300; \Sigma_g^+\rangle$	1278.35	3.908
$\|6; 300; \Sigma_g^+\rangle \to \|6; 300; \Sigma_g^+\rangle$	1393.14	1.595	$\|6; 300; \Sigma_g^+\rangle \to \|6; 220; \Sigma_g^+\rangle$	1374.59	0.0171
$\|4; 120; \Sigma_g^+\rangle \to \|6; 300; \Sigma_g^+\rangle$	1394.47	1.055	$\|4; 120; \Sigma_g^+\rangle \to \|6; 140; \Sigma_g^+\rangle$	1403.86	0.0590
$\|4; 120; \Sigma_g^+\rangle \to \|6; 140; \Sigma_g^+\rangle$	1427.86	1.646	$\|4; 040; \Sigma_g^+\rangle \to \|6; 060; \Sigma_g^+\rangle$	1429.32	0.1135
$\|6; 140; \Sigma_g^+\rangle \to \|8; 320; \Sigma_g^+\rangle$	1250.56	0.1672	$\|6; 060; \Sigma_g^+\rangle \to \|8; 160; \Sigma_g^+\rangle$	1234.88	0.3175
$\|6; 300; \Sigma_g^+\rangle \to \|8; 320; \Sigma_g^+\rangle$	1254.64	0.4888	$\|6; 140; \Sigma_g^+\rangle \to \|8; 240; \Sigma_g^+\rangle$	1248.	0.7269
$\|6; 300; \Sigma_g^+\rangle \to \|8; 400; \Sigma_g^+\rangle$	1265.41	0.4257	$\|6; 220; \Sigma_g^+\rangle \to \|8; 320; \Sigma_g^+\rangle$	1266.27	1.215
$\|6; 300; \Sigma_g^+\rangle \to \|8; 400; \Sigma_g^+\rangle$	1387.16	0.6370	$\|6; 300; \Sigma_g^+\rangle \to \|8; 320; \Sigma_g^+\rangle$	1362.5	0.0061
$\|6; 140; \Sigma_g^+\rangle \to \|8; 320; \Sigma_g^+\rangle$	1404.8	0.3841	$\|6; 220; \Sigma_g^+\rangle \to \|8; 240; \Sigma_g^+\rangle$	1395.26	0.0205
$\|6; 300; \Sigma_g^+\rangle \to \|8; 320; \Sigma_g^+\rangle$	1411.14	0.6627	$\|6; 140; \Sigma_g^+\rangle \to \|8; 160; \Sigma_g^+\rangle$	1424.53	0.0398

the energy distribution are responsible for the fine details shown in Figures 3 and 4.

Finally, in Figure 8, we present the simulation of the Raman spectrum provided by the P_{212} polyad for different temperatures. In order to see the differences in detail, in Figure 8 we show the predictions divided in two frequency ranges. In general, at temperature 100 K, only two peaks dominate the Raman spectrum. As the temperature augments to 300 K, the population of excited states increases appearing intensities around 1,285 and 1,390 cm^{-1} even with dominance over the intensities of higher temperature. With the exception of the previous transition lines, at temperatures higher than 1,000 K, the intensities of other transitions involving higher excited states increase

approaching the spectral lines to the results at T = 1,743 K. Raman predicted for temperatures 2,000 and 3,000 K are also displayed with similar behavior. This result shows a strong temperature intensity dependence at some frequencies.

4.1 | Intensity borrowing via Fermi resonance

In this section, we focus on the importance of the Fermi interaction for a correct description of the CO_2, which is common to the three polyads. Since its introduction by Fermi in 1931,[42] the Fermi interaction in CO_2 is a paramount example of a situation where a sole resonance or coupling is capable of improving dramatically a
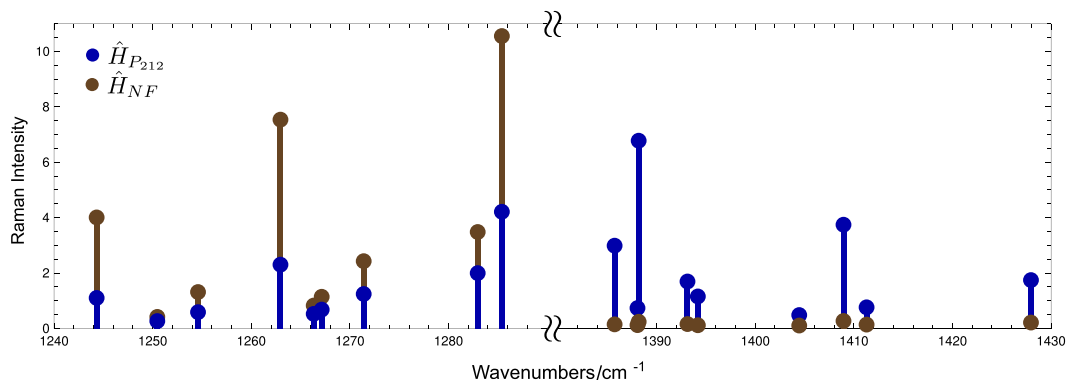
FIGURE 9 Raman intensities of transitions from Table 4 obtained using Hamiltonian $\hat{H}_{P_{212}}$ (17) (blue) and Hamiltonian $\hat{H}_{NF}$ (4.1) (brown)
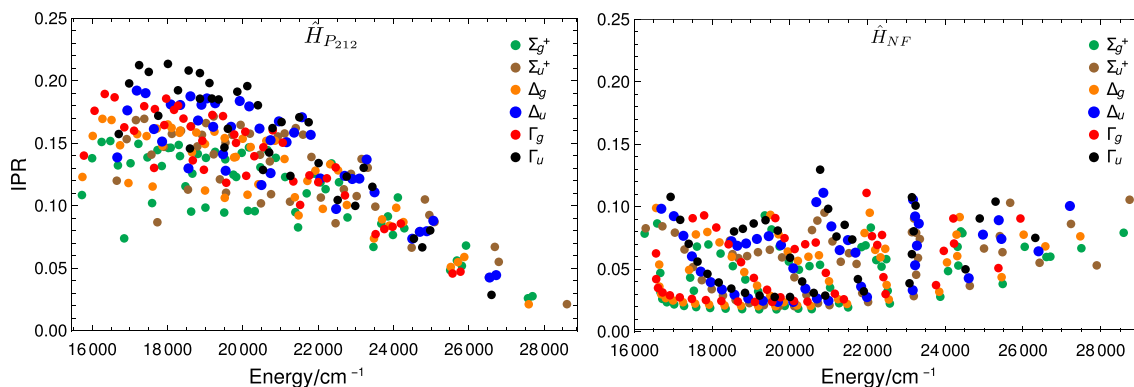

FIGURE 10 Inverse participation ratio as a function of the state energy for polyad 26 eigenstates and six different symmetries. States are obtained by diagonalization in the symmetry-adapted basis of Hamiltonian $\hat{H}_{P_{212}}$ (17) (left panel) and non-Fermi Hamiltonian $\hat{H}_{NF}$ (4.1) (right panel). Dot colors indicate the symmetry, as shown in the plot legend

molecular species spectroscopic description. For this reason, we include in this work some features of the Fermi resonance not discussed before. To illustrate the importance of the Fermi resonance, we consider the following Hamiltonian in the polyad scheme P_{212}

$$
\begin{aligned}
\hat{H}_{NF} = &\sum_{i=1}^{3} \omega_i \hat{v}_i + \sum_{i \leq j} x_{ij} \{\hat{v}_i, \hat{v}_j\} + g_{22}\hat{l}^2 \\
&+ x_{113}\{\hat{v}_1^2, v_3\} + x_{133}\{\hat{v}_1, \hat{v}_3^2\} + x_{123}\hat{v}_2\{\hat{v}_1, \hat{v}_3\} \\
&+ \alpha_1^s\{(\hat{n}_1 + \hat{n}_2), \hat{D}_L + 2\hat{n}_1\hat{n}_2\} + \alpha_2^{sb}\hat{n}(\hat{D}_L + 2\hat{n}_1\hat{n}_2) \\
&+ f_{uu/gg}[b_{\Sigma_g}^{+2} b_{\Sigma_u}^2 + H.c.],
\end{aligned}
\tag{39}
$$

where the three Fermi interactions have been neglected from Hamiltonian (17). We carry out a fit with this 16 parameter Hamiltonian to the 178 experimental vibrational levels, obtaining an *rms* = 25.76 cm^{-1}. As expected, it is mandatory to include the Fermi resonance in order to obtain a realistic description of CO_2, and the Hamiltonian terms that include the anharmonic resonances between bending and stretching modes are fundamental. In Table 4, we show the comparison of the Raman intensity obtained

for a selected set of transitions using Hamiltonians $\hat{H}_{P_{212}}$ (17) and H_{NF} (4.1). The conspicuous differences in transition labels and energies are explained taking into account that the fitting procedure is based on the minimization of energy differences with the experiment, without considering the quantum labels assignment. It is worth to notice that the value of the Raman intensities provided by the Hamiltonian $\hat{H}_{NF}$ (4.1) is higher than the ones from Hamiltonian $\hat{H}_{P_{212}}$ (17) for the lowest energy transitions in Table 4 (where transitions are ordered according to the polyad number), whereas the opposite occurs for the high energy states. This behavior is clearly seen in Figure 9, where the values of the transition frequencies were fixed to the experimental values in order to facilitate the comparison.

Additionally, the effect of the Fermi resonance on the vibrational wave functions can be assessed with the inverse participation ratio (IPR), a quantity that measures the level of localization of a quantum state in a given basis.[69] This quantity is closely related to the Shannon entropy,[70] and it has recently been used in algebraic models to characterize quantum phase transitions.[71] For a quantum state $|\Psi\rangle$ expressed in the basis $\{|i\rangle\}_{i=1}^{D}$, the IPR is defined as

$$|\Psi\rangle = \sum_{i=1}^{D} \alpha_i |i\rangle; \quad IPR_\Psi = \frac{1}{D \sum_{i=1}^{D} \alpha_i^4}, \tag{40}$$

where D is the basis dimension. An IPR value of 1 indicates a strongly mixed state, with all basis states participating in the state with equal components, whereas the minimum $1/D$ value is obtained for a $|\Psi\rangle$ state that has only one nonzero component.

We show in Figure 10 a scatterplot of IPR values versus state energies for a subset of polyad $P_{212} = 26$ eigenfunctions, with symmetry $\Sigma_g^+, \Sigma_u^+, \Delta_g, \Delta_u, \Gamma_g,$ or Γ_u. We compare the results for Hamiltonian $\hat{H}_{P_{212}}$ (17) in the left panel with non-Fermi Hamiltonian $\hat{H}_{NF}$ (4.1) in the right panel. The different colors indicate the different symmetry labels, as stated in the plot legend, and the dimension D depends on the symmetry. As expected, Hamiltonian $\hat{H}_{P_{212}}$ eigenstates have larger IPR values than Hamiltonian $\hat{H}_{NF}$ eigenstates, which indicates the stronger mixing due to the presence of the Fermi resonance. But also the qualitative behavior is different, with more localized states for higher energies in the $\hat{H}_{P_{212}}$ and an opposite behavior in the non-Fermi $\hat{H}_{NF}$ case.

5 | SUMMARY AND CONCLUSIONS

In this contribution, we present a high quality description of the CO_2 vibrational spectroscopy using the algebraic model $U_1(2) \times U(3) \times U_2(2)$. We compare the Raman spectrum simulated using wave functions obtained fitting the algebraic Hamiltonian to experimental data using the three different polyad schemes more frequently found in the literature for this particular molecular species, P_{212}, P_{213}, and P_{214}. The algebraic Hamiltonian is the same in the three cases except for the resonance operator that characterizes the polyad scheme (13), (14), and (15). We have carried out a detailed analysis of the effects of the different interactions included in the algebraic Hamiltonian. As regards the fit to experimental energy terms, we obtained a very good agreement with the data, and the final *rms* obtained with the three polyad schemes is similar $rms_{P_{212}} \simeq rms_{P_{213}} = 0.14 \text{ cm}^{-1}$, and $rms_{P_{214}} = 0.20 \text{ cm}^{-1}$.

The wave functions derived from the energy fits are evaluated through the simulation of the Raman spectrum. Apart from differences in the tails of the energy regions considered, the spectra for the three polyad schemes follow similar structures, which lead us to conclude that the Raman spectrum is mostly dictated by interactions common to the three polyad schemes.

For the three polyad schemes, the quality of the energy fits is similar to our previous results in Ref.,[11] and we have notably improved the calculated Raman intensities from Refs.[15,67]. As the number of transitions entering into the

Raman spectrum simulation is much larger in the present work, in order to elucidate the origin of the improvement in the calculated intensities, we have simulated the Raman spectrum with a reduced number of transitions, taking into account only those involved in the previous calculation. These results are shown in Figure 6 and demonstrate that the improvement is mostly due to the higher quality of the wave functions in the present work, although the larger number of considered transitions makes a difference mainly in the tails of the spectrum, with a significantly improved agreement with the experiment.

Another possible source of discrepancy with previous works could stem from the optimized partial derivatives of the polarizability. In order to clarify the importance of these quantities, we have modeled the CO_2 Raman spectrum using both previous and present work values for them. As shown in Figure 5, the spectrum structure turns out to be very similar.

Based on the previous arguments, we conclude that the resonances including the asymmetric stretching mode that define the three polyad schemes more frequently found in the literature are not relevant to obtain a good vibrational description in light of the simulations of the CO_2 Raman spectrum carried out in this work. The three polyads play similar roles because the truly necessary resonance is the Fermi interaction. However, in detail, the differences are manifested among the three polyad schemes due to anharmonic effects as well as energy distribution.

Finally, predictions of the Raman spectrum at temperatures T $= 100, 300, 1,000, 2,000,$ and $3,000 K$ were presented in Figure 8. In general, due to the increasing of excited states population, some intensity peaks increase with temperature.

ORCID

Renato Lemus [ID] https://orcid.org/0000-0002-9233-968X

REFERENCES

[1] D. Lüthi, M. Le Floch, B. Bereiter, T. Blunier, J.-M. Barnola, U. Siegenthaler, D. Raynaud, J. Jouzel, H. Fischer, K. Kawamura, T. F. Stocker, *Nature* **2008**, *453*, 379.

[2] J. M. Fernández, A. Punge, G. Tejeda, S. Montero, *J. Raman Spectrosc.* **2006**, *37*(1-3), 175.

[3] H. Ajrouche, A. Lo, P. Vervisch, A. Cessou, *Meas. Sci. Technol.* **2015**, *26*, 075501.

[4] L. B. d'Hendecourt, M. Jourdain de Muizon, *Res. Astron. Astrophys.* **1989**, *223*, 5.

[5] M. Sánchez-Castellanos, R. Lemus, M. Carvajal, F. Pérez-Bernal, *J. Mol. Spectrosc.* **2009**, *253*, 1.

[6] M. Sánchez-Castellanos, R. Lemus, M. Carvajal, F. Pérez-Bernal, *Int. J. Quantum Chem.* **2012**, *112*, 3498.

[7] A. Chedin, J. Teffo, *J. Mol. Spectrosc.* **1984**, *107*, 333.

[8] J. Zuñiga, M. Alacid, A. Bastida, F. Carvajal, A. Requena, *J. Mol. Spectrosc.* **1999**, *195*, 137.

[9] J. Zuñiga, A. Bastida, M. Alacid, A. Requena, *J. Mol. Spectrosc.* **2001**, *205*, 62.

[10] J. Cerezo, A. Bastida, A. Requena, J. Zuñiga, *J. Quant. Spectrosc. Radiat. Transf.* **2014**, *147*, 233.

[11] M. Bermudez-Montaña, R. Lemus, F. Pérez-Bernal, M. Carvajal, *Eur. Phys. J. D Atom. Mol. Opt. Phys.* **2017**, *71*, 147.

[12] M. E. Kellman, *J. Chem. Phys.* **1990**, *93*(9), 6630.

[13] A. McCoy, E. S. III, *J. Chem. Phys.* **1991**, *95*, 3476.

[14] B. Perevalov, S. Kassi, V. Perevalov, S. Tashkun, A. Campargue, *J. Mol. Spectrosc.* **2008**, *252*, 143.

[15] R. Lemus, M. Sánchez-Castellanos, F. Pérez-Bernal, J. M. Fernández, M. Carvajal, *J. Chem. Phys.* **2014**, *141*, 054306.

[16] A. R. Hoy, I. M. Mills, G. Strey, *Mol. Phys.* **1972**, *24*(6), 1265.

[17] D. Papousek, M. R. Aliev, *Molecular Vibrational-Rotational Spectra*, Elsevier, Amsterdam **1982**.

[18] P. Bunker, P. Jensen, *Molecular Symmetry and Spectroscopy*, NRC Research Press, Ottawa **1989**.

[19] R. Meyer, H. H. Gönthard, *J. Chem. Phys.* **1968**, *49*(4), 1510.

[20] H. M. Pickett, *J. Chem. Phys.* **1972**, *56*(4), 1715.

[21] E. Kauppi, L. Halonen, *J. Chem. Phys.* **1992**, *96*(4), 2933.

[22] M. Bermúdez-Montaña, R. Lemus, O. Castaños, *Mol. Phys.* **2017**, *115*(24), 3076.

[23] C. Amezcua-Eccius, R. Lemus, *J. Mol. Spectrosc.* **2010**, *260*(1), 36.

[24] M. Carvajal, R. Lemus, *J. Phys. Chem. A* **2015**, *119*, 12,823.

[25] R. Lemus, A. Frank, *J. Mol. Spectrosc.* **2000**, *201*, 198.

[26] A. Frank, R. Lemus, M. Carvajal, C. Jung, E. Ziemniak, *Chem. Phys. Lett.* **1999**, *308*, 91.

[27] M. Carvajal, R. Lemus, A. Frank, C. Jung, E. Ziemniak, *Chem. Phys.* **2000**, *260*, 105.

[28] R. Lemus, R. Bernal, *Chem. Phys.* **2002**, *283*, 401.

[29] R. Lemus, *J. Mol. Spectrosc.* **2004**, *225*, 73.

[30] R. Bernal, R. Lemus, *J. Mol. Spectrosc.* **2006**, *235*, 218.

[31] O. Álvarez-Bajo, M. Carvajal, F. Pérez-Bernal, *Chem. Phys.* **2012**, *392*, 63.

[32] A. Frank, R. Lemus, R. Bijker, F. Pérez-Bernal, J. M. Arias, *Ann. Phys.* **1996**, *252*, 211.

[33] R. Lemus, M. Carvajal, J. C. López-V, A. Frank, *J. Mol. Spectrosc.* **2002**, *214*, 52.

[34] M. Sánchez-Castellanos, C. Amezcua-Eccius, O. Álvarez-Bajo, R. Lemus, *J. Mol. Spectrosc.* **2008**, *247*, 140.

[35] F. Iachello, S. Oss, *J. Chem. Phys.* **1996**, *104*, 6996.

[36] F. Iachello, F. Pérez-Bernal, P. H. Vaccaro, *Chem. Phys. Lett.* **2003**, *375*, 309.

[37] F. Pérez-Bernal, L. Santos, P. Vaccaro, F. Iachello, *Chem. Phys. Lett.* **2005**, *414*, 398.

[38] F. Pérez-Bernal, F. Iachello, *Phys. Rev. A* **2008**, *77*, 032115.

[39] D. Larese, F. Iachello, *J. Mol. Spectrosc.* **2011**, *1006*(1), 611.

[40] D. Larese, F. Pérez-Bernal, F. Iachello, *J. Mol. Spectrosc.* **2013**, *1051*, 310.

[41] G. Herzberg, *Infrared and Raman Spectra of Polyatomic Molecules*, Van Nostrand, Princeton, NJ **1945**.

[42] E. Fermi, *Z. Phys.* **1931**, *71*, 250.

[43] M. Bermúdez-Montaña, R. Lemus, O. Castaños, *EPL (Europhysics Letters)* **2016**, *116*(1), 13001.

[44] Y. Tan, X.-Q. Zhao, A.-W. Liu, S.-M. Hu, O. Lyulin, S. Tashkun, V. Perevalov, *J. Quant. Spectrosc. Radiat. Transf.* **2015**, *165*, 22.

[45] T. Petrova, A. Solodov, A. Solodov, O. Lyulin, Y. Borkov, S. Tashkun, V. Perevalov, *J. Quant. Spectrosc. Radiat. Transf.* **2015**, *164*, 109.

[46] D. Jaquemart, Y. Borkov, O. Lyulin, S. Tashkun, V. Perevalov, *J. Quant. Spectrosc. Radiat. Transf.* **2015**, *160*, 1.

[47] E. Karlovets, S. Kassi, S. Tashkun, V. Perevalov, A. Campargue, *J. Quant. Spectrosc. Radiat. Transf.* **2014**, *144*, 137.

[48] S. Tashkun, V. Perevalov, J. Teffo, L. Rothman, V. Tyuterev, *J. Quant. Spectrosc. Radiat. Transf.* **1998**, *60*(5), 785.

[49] S. A. Tashkun, V. I. Perevalov, J.-L. Teffo, V. G. Tyuterev, *J. Quant. Spectrosc. Radiat. Transf.* **1999**, *62*(5), 571.

[50] S. A. Tashkun, V. I. Perevalov, *J. Quant. Spectrosc. Radiat. Transf.* **2011**, *112*(9), 1403.

[51] K. Song, S. Kassi, S. Tashkun, V. Perevalov, A. Campargue, *J. Quant. Spectrosc. Radiat. Transf.* **2010**, *111*, 332.

[52] A. Campargue, K. F. Song, N. Mouton, V. I. Perevalov, S. Kassi, *J. Quant. Spectrosc. Radiat. Transf.* **2010**, *111*(5), 659.

[53] R. Lemus, *Mol. Phys.* **2003**, *101*, 2511.

[54] O. Álvarez-Bajo, R. Lemus, M. Carvajal, F. Pérez-Bernal, *Mol. Phys.* **2011**, *109*, 797.

[55] L. Rothman, R. Hawkins, R. Wattson, R. Gamache, *J. Quant. Spectrosc. Radiat. Transf.* **1992**, *48*, 537.

[56] A. Campargue, D. Bailly, J. Teffo, S. Tashkun, V. Perevalov, *J. Mol. Spectrosc.* **1999**, *193*, 204.

[57] G. Weireauch, G. Wumaier, A. Campargue, S. Tashkun, V. Perevalov, J. Teffo, *J. Mol. Spectrosc.* **1999**, *198*, 187.

[58] G. Weireauch, A. Campargue, *J. Mol. Spectrosc.* **2001**, *207*, 263.

[59] C. Miller, L. Brown, *J. Mol. Spectrosc.* **2004**, *228*, 329.

[60] S. Kassi, K. Song, A. Campargue, *J. Mol. Spectrosc.* **2009**, *110*, 1801.

[61] H. Ishikawa, H. Toyosaki, N. Mikami, F. Pérez-Bernal, P. Vaccaro, F. Iachello, *Chem. Phys. Lett.* **2002**, *365*(1-2), 57.

[62] G. Tejeda, B. Maté, S. Montero, *J. Chem. Phys.* **1995**, *103*(2), 568.

[63] R. Akhmedzhanov, A. Atakhodzhaev, M. Bulanin, *J. Mol. Struct. (Thoechem)* **1982**, *89*(3-4), 285.

[64] G. Maroulis, *Chem. Phys.* **2003**, *291*(1), 81.

[65] A. Haskopoulos, G. Maroulis, *Chem. Phys. Lett.* **2006**, *417*(1-3), 235.

[66] M. Chrysos, I. A. Verzhbitskiy, F. Rachet, A. P. Kouzov, *J. Chem. Phys.* **2011**, *134*(10), 104,310.

[67] M. Sánchez-Castellanos, R. Lemus, M. Carvajal, F. Pérez-Bernal, J. M. Fernández, *Chem. Phys. Lett.* **2012**, *554*, 208.

[68] M. Carvajal, C. Favre, I. Kleiner, C. Ceccarelli, E. Bergin, D. Fedele, *Res. Astron. Astrophys.* **2019**, *627*, A65.

[69] F. Evers, A. D. Mirlin, *Rev. Mod. Phys.* **2008**, *80*, 1355.

[70] V. Zelevinsky, B. A. Brown, N. Frazier, M. Horoi, *Phys. Rep.* **1996**, *276*, 85.

[71] L. F. Santos, F. Pérez-Bernal, *Phys. Rev. A* **2015**, *92*, 050101.

SUPPORTING INFORMATION

Additional supporting information may be found online in the Supporting Information section at the end of the article.